ISSN 1330-3651 (Print), ISSN 1848-6339 (Online) https://doi.org/10.17559/TV-20220828050652
Original scientific paper

Study on Magnetic Field Modeling and Transmission Performance of Radial Solid Permanent Magnet Coupler

Junyue YANG*, Yanjun GE

Abstract: In order to study the magnetic field model and transmission characteristics of radial solid permanent magnet coupler deeply, an 11 kW experimental prototype of solid permanent magnet coupler is taken as the object, its operation principle is analyzed in detail, and based on moving magnetic field theory and transient eddy current equation, a complete magnetic field model is established by finite element difference method, distribution of electromagnetic field is solved and the mechanical characteristics curve is drawn, the rated torque, starting torque and maximum torque of the experimental prototype are obtained, operating parameters of the experimental prototype meet the design objectives and have certain overload protection functions. Based on the theory analysis, the structural design and processing assembly of the experimental prototype are completed. An experimental platform was built, the correctness of electromagnetic torque calculation process was verified by dynamic loading experiments. Furthermore, the fluctuating load buffering experiment was performed, and the load fluctuation was reduced to 30%, which proved the flexible transmission characteristics and impact relieved function.

Keywords: electromagnetic torque; finite element difference model; radial solid permanent magnet coupler; relieve impact efficiency; transmission characteristics

1 INTRODUCTION

As a novel torque transmission device, permanent magnet coupler conduct non-contact torque transmission by magnetic field coupling principle. It reduces disadvantages of noise, vibration, friction and wear caused by traditional transmission technology [1, 2], and has advantages such as cleaning, high efficiency and energy saving [3, 4], so permanent magnet coupler has wide application prospect [5].

At present, many scholars have made some achievements in this technology. Wallace et al. [6] proposed a structure of disk type permanent magnet coupler, in which the magnetic field generated by the permanent magnet rotating under the driving shaft cuts the conductor disk, generates eddy currents on the conductor disk to form a reactive magnetic field, and achieves rotational driving through the coupling effect of the magnetic field. Canova et al. [7] studied the design method of axial permanent magnet coupler, conducted theoretical analysis using Variable Separation Method (VSM), established two-dimensional and three-dimensional magnetic field models, and conducted detailed research on operating parameters. Canova et al. [8] proposed the structure of a radial asynchronous magnetic coupling, extended it to a double-layer permanent magnet structure, and optimized the structural parameters to determine their impact on electromagnetic torque. Cha et al. [9] investigated the different magnetization directions influence of permanent magnets on the electromagnetic torque, and analyzed and calculated the magnetic field of structures with different magnetization directions by finite element analysis. Sajjad et al. [10] constructed an experimental prototype of disk permanent magnet coupling and analyzed it by three-dimensional finite element method. Lubin et al. [11] derived the output torque calculation model of disk type magnetic coupler under condition of small speed difference by Maxwell stress tensor method, and analyzed transmission performance of magnetic coupler under static and transient conditions. Ge et al. [12] proposed a magnetic coupler with a squirrel cage structure, and analyzed magnetic field model and transmission characteristics. Vahid et al. [13] obtained optimal parameter combination of permanent magnet disk and conductor disk and established a steady-state model. Yang et al. [14] took a slotted disk magnetic coupler as research object, and used finite element software to simulate the mechanical characteristic curve, speed regulation characteristic curve and power characteristic curve. Yang et al. [15] proposed a structure of radial permanent magnet coupling with an outer cage rotor, derived electromagnetic torque equation by magnetic circuit method, and conducted in-depth research on electromagnetic torque, transmission efficiency, and heat generation of this structure.

In addition, many enterprises have also invested in the industrial application of magnetic couplers. Magna Drive Company has developed a disc type magnetic coupler with speed regulation function and conducted application experiments on industrial sites, which has functions such as soft start and speed regulation [16]. The axial permanent magnet coupler products produced by Magna Magnetic Power Co. Ltd. are applied in industrial fields such as metallurgy, mining, petrochemicals and power, with transmission power of up to 500 kW [17].

In conclusion, permanent magnet couplers are mainly divided into axial (disc) permanent magnet couplers and radial (cylindrical) permanent magnet couplers according to their structural forms. The development of axial permanent magnet couplers was earlier (in 1995), it uses the induced eddy current magnetic field in copper discs to couple with the permanent magnet magnetic field for magnetic transmission, its structure is simple and has been applied in industry. But due to the limitation of magnetic saturation in air gap, the axial permanent magnet couplers need to increase the diameter in order to obtain a larger transmission torque, resulting in excessive rotational inertia of transmission system, so this structure is difficult to promote and apply in high-power equipment (above 500 kW). The research on radial permanent magnet couplers started relatively later (in 2005), this structural form can obtain a larger air gap magnetic field area by increasing the axial length of the rotor, so it can obtain a larger

electromagnetic torque with a smaller diameter, making it easier to achieve high-power applications.

According to the analysis of above, most research has focused on axial permanent magnet couplers, while research and development on radial permanent magnet couplers are relatively limited, especially in terms of magnetic field analysis and transmission characteristics. So an 11 kW radial solid permanent magnet coupler is taken as research object in this paper. Based on theory of string magnetic field and transient eddy current equations, a complete magnetic field model is established by finite element difference method, and the distribution of the electromagnetic field is analyzed in detail. On the basis of the above, a mechanical characteristic curve reflecting transmission performance was drawn, and an experimental platform was built to verify the theoretical analysis.

2 BASIC STRUCTURE AND WORKING PRINCIPLE

The basic structure of radial solid permanent magnet coupler includes permanent magnet outer rotor and conductor inner rotor, and there is a uniform air gap between them, as shown in Fig. 1.

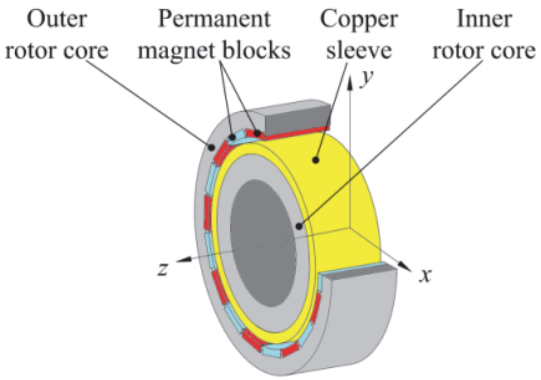

Figure 1 Basic structure of radial solid permanent magnet coupler

The permanent magnet outer rotor is composed of permanent magnet blocks and outer rotor core. The permanent magnet blocks are generally arc-shaped or rectangular blocks arranged in pairs along circumferential direction, they are magnetized in the radial direction, and the magnetization directions between adjacent two blocks are opposite. The outer rotor core is generally made of low-carbon steel, and permanent magnets are embedded on inner surface of the outer rotor core.

The conductor inner rotor is composed of inner rotor core and copper sleeve. The inner rotor core is also made of low carbon steel and the copper sleeve is generally made of red copper with high conductivity.

The working principle of radial solid permanent magnet coupler is shown in Fig. 2.

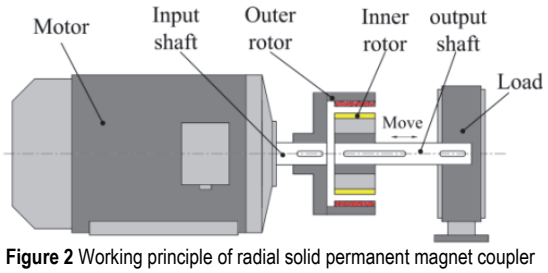

Figure 2 Working principle of radial solid permanent magnet coupler

In Fig. 2, the outer rotor is connected to motor as input end, and the inner rotor is connected to load as output end. Permanent magnetic field formed by permanent magnet blocks rotates with outer rotor and cuts copper sleeve, which generates induced electromotive force and eddy current in copper sleeve. Under action of Lorentz force, electromagnetic torque transmission between the inner and outer rotors is realized. The working process is a slip torque transmission, there is no mechanical contact, so transmission mode has flexible characteristics, which can greatly reduce the impact of load fluctuation on motor. Furthermore, speed regulating device can be designed to change coupling length between inner and outer rotors, which can realize stepless speed regulating function under certain conditions.

This paper focuses on transmission characteristics and reduces the impact of load fluctuation, so an 11 kW experimental prototype of fixed coupling length is designed and analyzed. The operating parameters of prototype include input speed is 1500 rpm, rated output speed is 1458 rpm, and rated torque is 72 Nm. The basic end face structure is shown in Fig. 3.

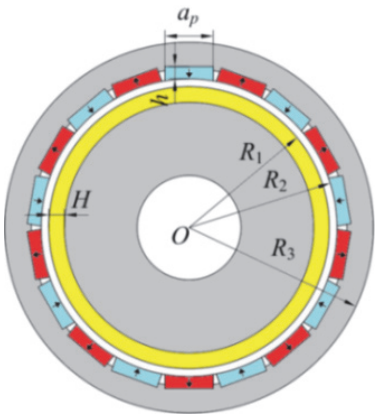

Figure 3 End face structure of experimental prototype

In Fig. 3, R_1 is outer radius of copper sleeve, R_2 is inner radius of permanent magnet block, R_3 is outer radius of outer rotor core, h is air gap length, a_p is width of permanent magnet block and H is thickness of copper sleeve.

The permanent magnet block is half tile type structure, inner surface is an arc surface, and surface embedded in outer rotor core is a plane. In order to ensure positioning of permanent magnet block in circumferential direction, inner surface of outer rotor core is an uniform groove structure, so there is a certain gap between permanent magnet blocks. The copper sleeve is pressed on the inner rotor core by interference. The dimensions parameters are shown in Tab. 1.

The material parameters are shown in Tab. 2.

Table 1 Basic structural dimensions of prototype

Structural parameters	Value
Pole pairs of permanent magnets	9
Outer radius of outer rotor/ mm	177,5
Inner radius of outer rotor / mm	142,5
Thickness of permanent magnet / mm	15
width of permanent magnet / mm	47,6
Outer radius of inner rotor / mm	141,5
Inner radius of inner rotor / mm	60
Axial coupling length / mm	60
Air gap length / mm	1

Table 2 Material parameters of prototype

Material parameters	Value
Outer and inner rotor core	Q235
Permanent magnet material	NdFe35
copper sleeve material	Cu-ETP

3 MAGNETIC FIELD ANALYSIS

Based on moving magnetic field theory, according to Fig. 3, the radial solid magnetic coupler is expanded along air gap surface, as shown in Fig. 4.

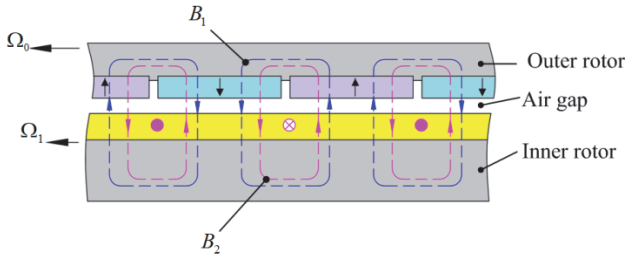

Figure 4 Magnetic circuit analysis

As shown in Fig. 4, under load state, mechanical angular velocity of outer rotor rotation is Ω_0, mechanical angular velocity of inner rotor rotation is Ω_1, $\Omega_0 \geq \Omega_1$, and slip difference between the inner and outer rotors Ω_s can be expressed as Eq. (1).

$$\Omega_S = \Omega_0 - \Omega_1 = (n_0 - n_1) \cdot R_1 \quad (1)$$

where, n_0 is rotation speed of outer rotor and$n_1$is rotation speed of inner rotor.

In Fig. 4, B_1 is magnetic induction intensity provided by permanent magnet blocks, B_2 is reactive magnetic induction intensity produced by induced current in copper sleeve. The synthetic magnetic induction intensity B_m is formed by superposition of B_1 and B_2.

As shown in Fig. 4, the magnetic fields are coupled and interact with each other, B_m rotates synchronously with outer rotor, due to slip difference between the inner and outer rotors, induced current are generated in the copper sleeve, which generates the reactive magnetic induction intensity B_2, B_2 reacts on B_m, and affecting B_1 at working point of permanent magnet block. It is difficult to directly calculate magnetic field distribution by analytical method, so the magnetic field model of finite difference method is established in this paper and solved by the iterative method of successive linearization.

3.1 Magnetic Field Model

According to structure shown in Fig. 3, the magnetic field of radial solid permanent magnet coupler can be analyzed as a two-dimensional field. Fig. 5 shows end face structure of one pair of poles.

Take Fig. 5 as solution domain, shape of boundary and interface is irregular, and distribution of ferromagnetic medium and current carrying conductor is complex. Considering magnetic saturation, a nonlinear magnetic field model under load can be established and solved by finite difference method. The solution domain A-B-C-D can be divided into 5 domains according to material properties. Domain I is outer rotor core, domain II is permanent magnet block, domain III is air gap area, domain IV is copper sleeve area and domain V is inner rotor core.

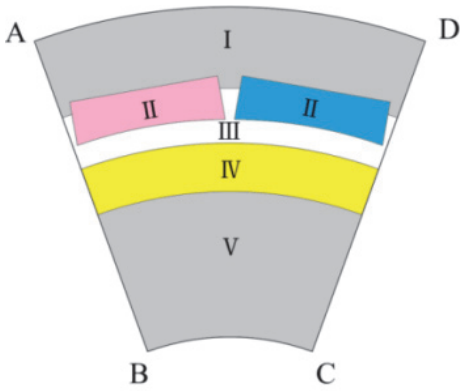

Figure 5 End face structure of one pair of poles

Domain I and domain V are soft magnetic materials, under magnetic saturation condition, relationship between magnetic reluctivity and magnetic induction intensity is nonlinear. According to material properties, relationship between magnetic reluctivity v and magnetic induction intensity B can be shown in Fig. 6.

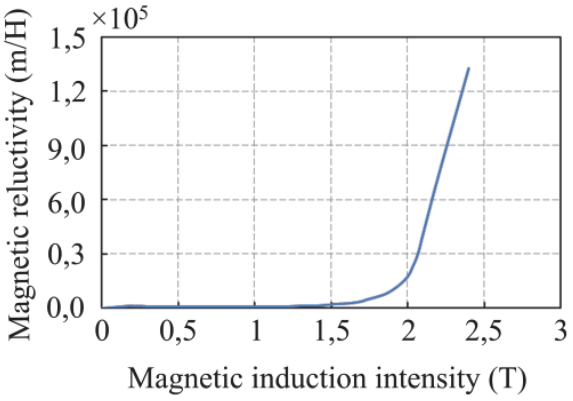

Figure 6 Relationship between magnetic reluctivity and magnetic induction intensity

Domain II is permanent magnet block, the magnetic reluctivity v_{II} = 7,96 × 10^5 m/H and its demagnetization curve in working state is shown in Fig.7.

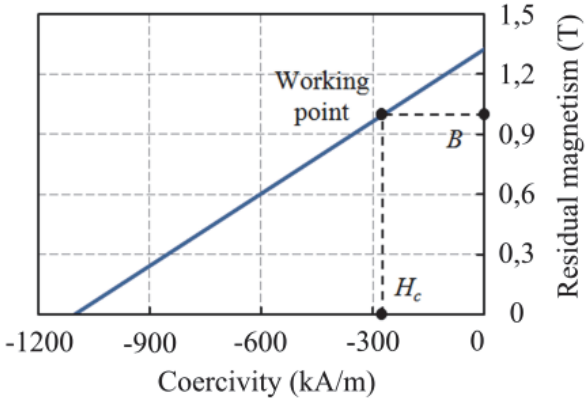

Figure 7 Demagnetization curve of permanent magnet block

In Fig. 7, the working point of permanent magnet block can be determined by magnetic induction intensity B according to intersection of demagnetization curve.

Domain III is air gap, the magnetic reluctivity of air is v_{III} = 7,96 × 10^5 m/H, it is conversion region of magnetic field energy.

Domain IV is copper sleeve, the magnetic reluctivity is v_{IV} = 7,96 × 10^5 m/H. Under load condition, induced electromotive force E will be generated in domain IV, and a reactive magnetic field will be generated to weaken magnetic field of permanent magnet. According to theory of moving magnetic field, induced electromotive force E can be expressed by Eq. (2):

$$\mathbf{rot}E = \sigma \mathbf{rot}J = -\frac{\partial B}{\partial t} + \mathbf{rot}\left(\Omega_S \times B\right) \tag{2}$$

where, σ is electrical resistivity, σ = 1,75 × 10^{-8} Ωm, J is current density, t is time, **rot** is curl symbol.

The interface conditions of different domain can be determined according to principle of magnetic field refraction, as shown in Eq. (3).

$$\left.\begin{aligned} \mu_1 H_1 \cos\theta_1 &= \mu_2 H_2 \cos\theta_2 \\ H_1 \sin\theta_1 &= H_2 \sin\theta_2 \end{aligned}\right\} \tag{3}$$

where, μ_1 and μ_2 are magnetic permeability of two media at the boundary, H_1 and H_2 are magnetic field intensity of two media at boundary, θ_1 and θ_2 are angle between magnetic induction intensity and interface direction in two media.

The vector magnetic potential A can be introduced, as shown in Eq. (4).

$$B = \mathbf{rot}A \tag{4}$$

Since solution domain is a two-dimensional field, only the components in z direction A_z are considered, and the boundary conditions of solution domain can be expressed by Eq. (5):

$$\left.\begin{aligned} A_Z\big|_{AD} &= A_Z\big|_{BC} = 0 \\ A_Z\big|_{AB} &= A_Z\big|_{CD} \end{aligned}\right\} \tag{5}$$

And the two-dimensional nonlinear transient eddy current equation can be expressed by Eq. (6).

$$\frac{\partial}{\partial x}\left(v\frac{\partial A_z}{\partial x}\right) + \frac{\partial}{\partial y}\left(v\frac{\partial A_z}{\partial y}\right) = -J \tag{6}$$

3.2 Mesh Generation and Difference Separation

Make equidistant grid division in x direction of solution domain A-B-C-D, 36 grid lines, and make unequal grid division in y direction. There are 27 grid lines in total, 5 in domain I, 3 in domain II, 8 in domain III, 6 in domain IV, and 5 in domain V. So there are 972 nodes in total, all nodes are numbered with (i, j), and difference equation can be expressed by Eq. (7).

$$\begin{aligned} F_{i,j} = {} & L_{i,j}A_{i-1,j} + R_{i,j}A_{i+1,j} + B_{i,j}A_{i,j-1} + T_{i,j}A_{i,j+1} - \\ & - D_{i,j}A_{i,j} \end{aligned} \tag{7}$$

where, $L_{i,j}$, $R_{i,j}$, $B_{i,j}$, $T_{i,j}$ are left, right, upper and lower coefficients of magnetic potential (i, j), $D_{i,j}$ is coefficients of magnetic potential (i, j), $F_{i,j}$ is the value of electric density (i, j), they can be determined by Eq. (8).

$$\left.\begin{aligned} F_{i,j} &= -\frac{1}{4}(J_{i,j}h_i k_j + J_{i,j+1}h_i k_{j+1} \\ &\quad + J_{i+1,j+1}h_{i+1}k_{j+1} + J_{i+1,j}h_{i+1}k_j) \\ L_{i,j} &= \frac{v_{i,j}k_j + v_{i,j+1}k_{j+1}}{2h_i} \\ R_{i,j} &= \frac{v_{i+1,j}k_j + v_{i+1,j+1}k_{j+1}}{2h_{i+1}} \\ B_{i,j} &= \frac{v_{i,j}h_j + v_{i+1,j}h_{j+1}}{2k_j} \\ T_{i,j} &= \frac{v_{i,j+1}h_j + v_{i+1,j+1}h_{j+1}}{2k_{j+1}} \\ D_{i,j} &= L_{i,j} + R_{i,j} + B_{i,j} + T_{i,j} \end{aligned}\right\} \tag{8}$$

where, h_i and k_j are the x and y-direction step (i, j).

A set of nonlinear equations about nodes magnetic potential A_z can be established as Eq. (9)

$$KA = F \tag{9}$$

where, K is magnetic resistance coefficient matrix of medium and F is column vector of current density.

3.3 Calculation and Result Analysis

The Eq. (9) can be solved by successive linearization method, main steps can be as follows.

Step 1: For nonlinear equations shown in Eq. (9), the iterative scheme shown in Eq. (10) is constructed.

$$K(v^{(k)})A^{(k+1)} = F, \quad k = 0,1,2\ldots\ldots \tag{10}$$

where, k is the number of iterations.

Step 2: Assign initial values $v^{(0)}{}_{i,j}$ to magneto resistance at nodes of each domain (domain II, domain III and domain IV are non ferromagnetic regions, v=v_0, domain I and domain V are ferromagnetic regions, the magnetic resistance can be determined by the curve in Fig. 6), so a linear equation system about A can be shown as Eq. (11).

$$K(v^{(0)})A^{(1)} = F \tag{11}$$

Step 3: The first approximation value $A^{(1)}$ of magnetic phase sequence vector of each node can be calculated by solving Eq. (10) with line over relaxation iteration method.

Step 4: According to $A^{(1)}$, magnetic induction intensity B of each domain can be determined by center difference quotient method, as shown in Eq. (12).

$$\left.\begin{aligned} B &= \sqrt{B_x^2 + B_y^2}, \qquad i > 1, j > 1 \\ B_x &= \frac{1}{2}\left(\frac{u_{i,j} - u_{i,j-1}}{k_j} + \frac{u_{i-1,j} - u_{i-1,j-1}}{k_j}\right) \\ B_y &= \frac{1}{2}\left(\frac{u_{i,j} - u_{i-1,j}}{h_i} + \frac{u_{i,j-1} - u_{i-1,j-1}}{h_i}\right) \end{aligned}\right\} \tag{12}$$

where, $u_{i,j}$ is magnetic potential boundary value at node (i, j).

Step 5: According to B calculated by Eq. (10), the magnetic resistance correction value $v^{(1)}$ of each node can be determined according to $v = f(B)$ curve shown in Fig. 6, and working point of permanent magnet can be determined according to demagnetization curve shown in Fig. 7.

Step 6: Recalculate coefficients of Eq. (9) with corrected $v^{(1)}$, solve the corrected linear equations with iterative method, and obtain the second correction value $A^{(1)}$ of magnetic potential of each node,

Step 7: Repeat the above steps until difference between $A^{(k)}$ and $A^{(k+1)}$ is less than the set error (1%), then the iterative process can be considered to converge, and the value of last iteration is final solution.

According to calculation method above, vector magnetic potential A of each node under different slip speeds can be calculated, and distribution curve of magnetic force line can be shown as Fig. 8.

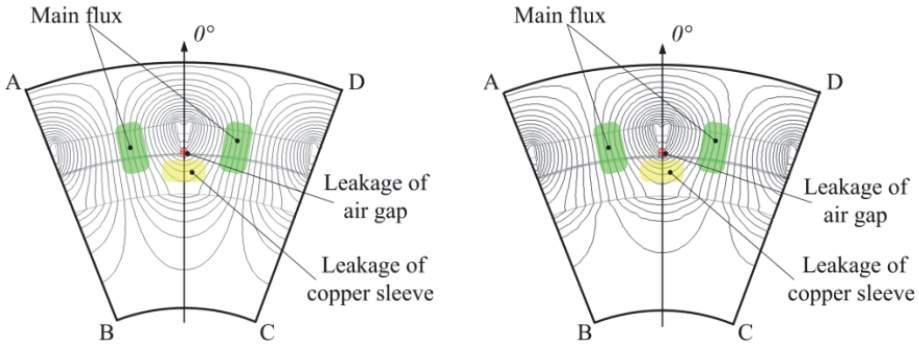

a) Inner rotor speed at 1500 rpm b) Inner rotor speed at 1460 rpm

Figure 8 Magnetic force line distribution under different speed of inner rotor

In Fig. 8, A_z = 150 × 10^{-3} Wb/m is the maximum equipotential curve, and an equipotential line is made with every 15 × 10^{-3} Wb/m magnetic potential difference.

As shown in Fig. 8, under different speed of inner rotor, the magnetic force line distribution of each pole pair can be divided into three parts according to different magnetic flux loop and functions. The loop of main flux is "permanent magnet block—air gap—copper sleeve—inner rotor core—copper sleeve—air gap—permanent magnet block—outer rotor core—permanent magnet block", the main magnetic flux passes through copper sleeve layer and its radial component generates induced electromotive force and electromagnetic torque in the copper sleeve. The loop of copper sleeve leakage is "permanent magnet block—air gap—copper sleeve—air gap—permanent magnet block outer rotor core—permanent magnet block", The leakage the copper sleeve does not completely penetrate the copper sleeve, and its tangential component accounts for a large proportion, which has a small impact on the generation of induced electromotive force and electromagnetic torque. The air gap leakage flux loop is "permanent magnet block—air gap—permanent magnet block—outer rotor core—permanent magnet block", due to small length of air gap, its influence on electromagnetic torque is neglected in this paper.

In Fig. 8a, the rotation speed of inner rotor is 1500 rpm, which is the same as that of outer rotor, it is no-load state, composite magnetic field is only generated by permanent magnet magnetic field, and magnetic force lines of each part are evenly distributed. In Fig. 8b, the rotation speed of the inner rotor is 1460 rpm, so there is a slip speed of 40 rpm with outer rotor, it is load state, a certain reaction electromotive force is generated in copper sleeve, which has a impact on magnetic flux circuit, and compared with Fig. 8a, magnetic force line of each part has a certain deformation.

According to Eq. (9), current density distribution in solution domain is solved, as shown in Fig. 9.

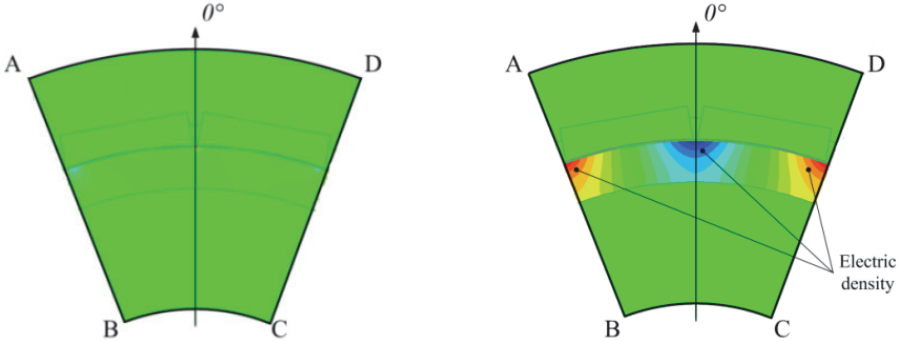

a) Inner rotor speed at 1500 rpm b) Inner rotor speed at 1460 rpm

Figure 9 Current density distribution under different speed of inner rotor

Fig. 9a and b are current density distribution under condition that inner rotor speed is 1500 rpm and 1460 rpm respectively. In Fig. 9a, it is no-load state, induced electromotive force and induced current are not generated in each part of solution domain. In Fig. 9b, it is load state, the electric density is mainly distributed at junctions of permanent magnet blocks (Maximum electric density is $1{,}26 \times 10^7$ A/m^2), and a reactive electromotive force is generated in copper sleeve, which weakens the radial component of magnetic flux and enhances the tangential component of the magnetic flux.

According to Eq. (10), magnetic induction intensity in air gap under different slip speeds can be calculated, as shown in Fig. 10 and Fig. 11.

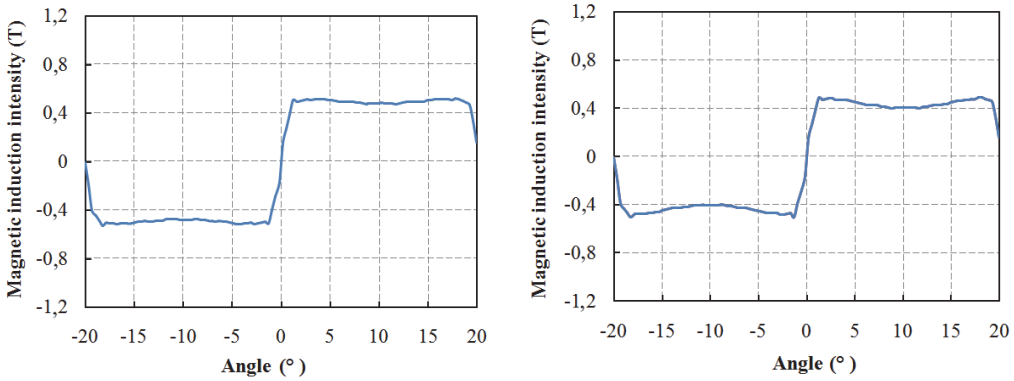

a) Inner rotor speed at 1500 rpm b) Inner rotor speed at 1460 rpm

Figure 10 Radial component of air gap magnetic induction intensity under different speed of inner rotor

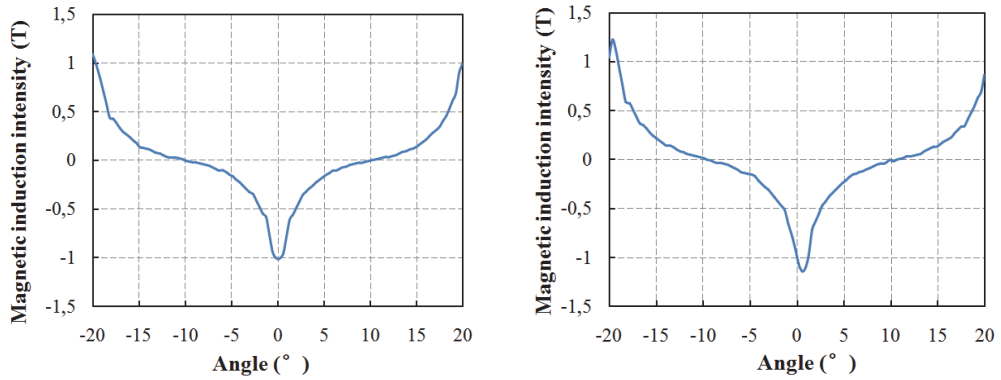

a) Inner rotor speed at 1500 rpm b) Inner rotor speed at 1460 rpm

Figure 11 Tangential component of air gap magnetic induction intensity under different speed of inner rotor

In Fig. 10a and b are radial component of air gap magnetic induction intensity under condition that inner rotor speed is 1500 rpm and 1460 rpm respectively. The average value in Fig. 10a is 0,48 T, and the average value in Fig. 10b is 0,41 T, the reactive magnetic field weakens the radial component of air gap magnetic field by 14,5%.

In Fig. 11a and b are tangential component of air gap magnetic induction intensity under condition that inner rotor speed is 1500 rpm and 1460 rpm respectively. The average value in Fig. 11a is 0,26 T, and the average value in Fig. 11b is 0,30 T, the reactive magnetic field enhances the tangential component of air gap magnetic field by 15,3%, and the overall offset is 0,9°.

According to Maxwell's stress tensor theory, electromagnetic torque can be expressed as Eq. (13):

$$T = \frac{LR_1^2}{\mu_0}\int_0^{2\pi}(B_r B_\theta)\mathrm{d}\theta \tag{13}$$

According to Eq. (12), when output speed is 1458 rpm, electromagnetic torque is 72 Nm

By changing speed of inner rotor, electromagnetic torque at different output speeds can be obtained, and relationship between electromagnetic torque and output speed can be shown as Fig. 12.

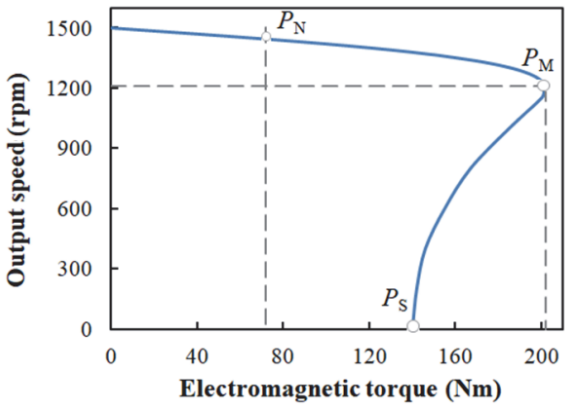

Figure 12 Relationship between electromagnetic torque and output speed

The curve shown in Fig. 12 is also mechanical characteristic curve of radial solid permanent magnet coupler, inflection point P_M corresponds to the maximum electromagnetic torque (201,4 Nm), and the critical speed (1210 rpm). Point P_S corresponds to starting torque (140,5 Nm). According to stability principle of electric drive system, for constant torque or constant power load, stable area is above critical speed. Rated working point of prototype point P_N (1458 rpm, 72 Nm) is within the stable range, which can meet design requirements.

4 EXPERIMENT AND RESULT ANALYSIS

On basis of theoretical analysis, a complete mechanical structure of radial solid permanent magnet coupler is designed and manufactured, main components and assembled prototype are shown in Fig. 13.

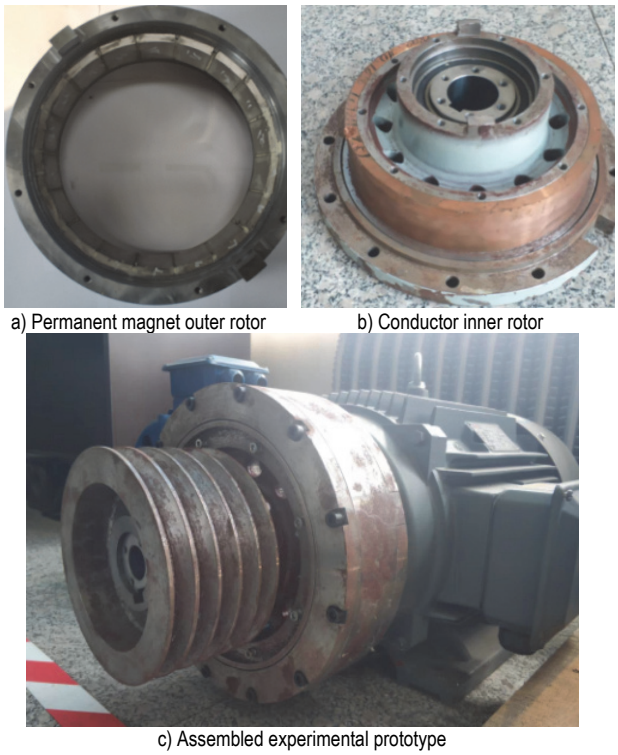

a) Permanent magnet outer rotor b) Conductor inner rotor

c) Assembled experimental prototype

Figure 13 Main components and assembled prototype

Experimental platform is built as shown in Fig. 14, which mainly include drive motor (Y2-160-4M), torque sensor (model: JD20, range: 0~1000 Nm, accuracy: 0,2%), loading motor (YP2-280-4M).

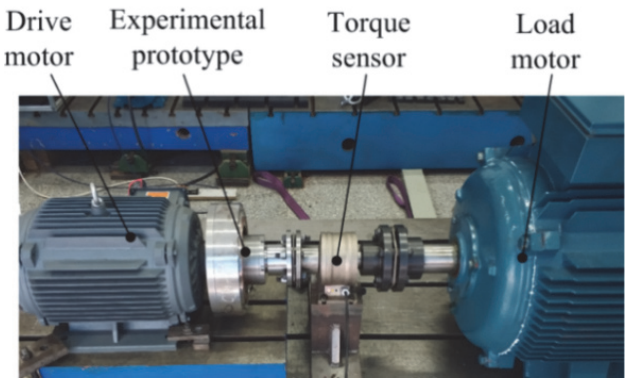

Figure 14 Experimental platform

The output shaft of drive motor is connected with outer rotor, and rotation speed is constant at 1500 rpm. The load torque of radial solid permanent magnet coupler can be controlled by changing the current of the load motor. The output torque and speed under different load conditions are read by torque sensor, relationship curve of "speed-torque" can be obtained, and compare experimental curve with theoretical curve, as shown in Fig. 15.

Because load is under constant torque condition, test points are all detected within the stable area. In Fig. 15, experimental curve and theoretical curve have good consistency. At the same speed, the maximum torque error is less than 3%, which verifies the correctness of the theoretical calculation, but experimental value is always slightly higher than theoretical value, this is because parameters of permanent magnet material (In Fig. 7) are selected according to lower limit of brand standard in theoretical calculation. Compared with standard 11kw asynchronous motor (Y2-160-4M, Rated speed: 1459 rpm, Rated torque: 72 Nm, Starting torque: 149,7 Nm, Maximum torque: 213,1 Nm), the parameters of experimental prototype are slightly lower (Rated speed: 1458 rpm, Rated torque: 72 Nm, Starting torque: 144 Nm, Maximum torque: 202 Nm), but this situation can meet normal working requirements of motor and provide certain overload protection.

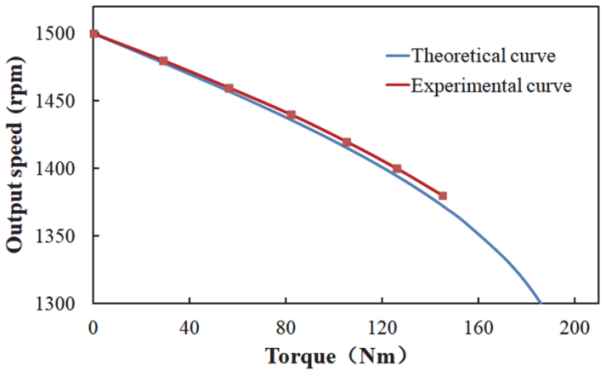

Figure 15 Relationship curve of "speed-torque"

To verify impact relieved function of prototype, at speed of outer rotor is constant at 1500 rpm, different fluctuating torques are applied to load end, as shown in Fig. 16.

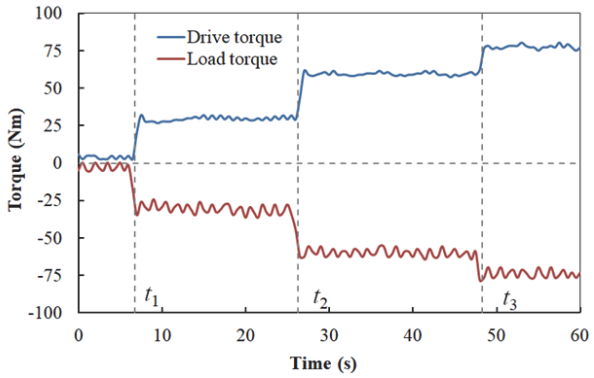

Figure 16 Drive torque and load torque under fluctuating load

In Fig. 16, at time 0, t_1, t_2 and t_3, average load torque is 5 Nm, 30 Nm, 60 Nm and 75 Nm, and fluctuation range of load is 10 Nm. The drive torque is the torque output by the motor shaft. Compare drive torque and load torque, because of working mode of air gap magnetic field flexible transmission, driving torque slightly lags behind load torque, and torque fluctuation is less than 3 Nm, which is only 30% of load fluctuation, which proves impact relieved function of the prototype.

5 CONCLUSION

An 11 kW radial solid permanent magnet coupler prototype is taken as research object in this paper,

according to string magnetic field theory and transient eddy current equation, finite element difference model of electromagnetic field is established, and magnetic field is analyzed in detail. The correctness of model and analysis is verified by experiments.

In the magnetic flux circuit, the copper sleeve area is a non-magnetic area, so the magnetic induction intensity in the air gap is weak, under the rated state, its radial magnetic induction intensity is 0,41 T, which is lower than the average air gap magnetic induction intensity of asynchronous motor (0,79 T), and air gap magnetic induction density is easily disturbed by load changes, which decreases by 14,5 % from no-load state to rated load. While, under the rated load, the lower air gap magnetic induction intensity leads to the highest electric density of the induced eddy current field in copper sleeve reaching $1{,}26 \times 10^7$ A/m^2, which is higher than electric density in rotor bar of asynchronous motor ($0{,}37 \times 10^7$ A/m^2), this eddy current is the main source of heat generation, so the effective magnetic flux area should be fully considered in the design process to reduce the excessive electric density in the copper sleeve, and the heat dissipation structure should be reasonably designed.

Compared with the 11 kW asynchronous motor, the mechanical characteristics of radial solid permanent magnet coupler are equivalent to those of the asynchronous motor within the rated load range, and the slip changes of both are 0,028. But, under the condition of starting with load, the starting torque of radial solid permanent magnet coupler (144 Nm) is slightly less than that of asynchronous motor (149,7 Nm), which ensures that if the load torque exceeds the starting torque of the motor, the motor and coupler will start and rotate by themselves first, then gradually drive the load, which is the soft start function. And the maximum torque of radial solid permanent magnet coupler (202 Nm) is also slightly less than the maximum torque of the asynchronous motor (213,1 Nm), which ensures that under the condition of overload, the coupler will produce slip phenomenon, so as to protect the motor and electrical equipment, that is the overload protection function.

The experimental results show that radial solid permanent magnet coupler has a lag effect in the process of transmitting fluctuating load, and the fluctuation amplitude is reduced to 30%, which effectively isolates the load fluctuation and protects the electrical circuit and mechanical components.

The working principle of radial solid permanent magnet coupler is slip transmission, it has characteristics of flexible transmission, but at cost of losing some efficiency. In the next work, the transmission efficiency will be focus of research.

Acknowledgement

This research is supported by National Natural Science Foundation of China (No. 51375063), Liaoning Science and Technology Planning Project (No. 2021-KF-14-05), Scientific Research Project of Liaoning Provincial Department of Education (No. LJKZ0499). All support is gratefully acknowledged.

6 REFERENCES

[1] Wallace, A. & Jouanne, A. V. (2001). Industrial Speed Control: PM Couplings an Alternative to VFDs. *IEEE Industry Applications Magazine*, *7*(5), 57-63. https://doi.org/10.1109/2943.948533

[2] Hwang, Y. J. & Jang, J. Y. (2020), Design and analysis of a novel magnetic coupler of an in-wheel wireless power transfer system for electric vehicles. *Energies*, *13*(2), 1-22. https://doi.org/10.3390/en13020332

[3] Duan, X. W. & Wang, X. D. (2012). Comparative Analysis of Speed Regulation and Energy Saving Methods of High-power Fan and Water pump. *Energy Conservation*, *31*(5), 28-31. https://doi.org/10.3969/j.issn.1004-7948.2012.05.008

[4] Zhao, G. X., Ma, W. J., & Cao, Y. G. (2010). Energy Saving Transformation of Permanent Magnet Speed Regulating Driver in Closed Cooling Water Pump. *Energy Conservation*, *29*(4), 41-44. https://doi.org/10.3969/j.issn.1004-7948.2010.04.010

[5] Zhu, J. H. (2014). Experimental Research on Energy-Saving Application of Permanent Magnet Speed Regulation Technology. *Applied Mechanics and Materials*, *694*, 242-246. https://doi.org/10.4028/www.scientific.net/AMM.694.242

[6] Wallace, A., Wohlgemuth, C., & Lamb, K. (1995). A high efficiency, alignment and vibration tolerant, coupler using high energy-product permanent magnets. *IEE Seventh International Conference on Electrical Machines and Drives - Durham*,11-13. https://doi.org/10.1049/cp:19950869

[7] Canova, A. & Vusini, B. (2003). Design of Axial Eddy-Current Couplers. *IEEE Transactions on Industry Applications*, *39*(3), 725-733. https://doi.org/10.1109/ias.2002.1043795

[8] Canova, A., Freschi, F., Gruosso, G., & Vusini, B. (2005). Genetic optimisation of radial eddy current couplings. *COMPEL-The international journal for computation and mathematics in electrical and electronic engineering*, *24*(3), 767-783. https://doi.org/10.1108/03321640510598120

[9] Cha. H. R., Cho. H. W., & Lee, S-H. (2008) The influence of magnetization pattern on the performance of permanent magnet eddy current couplings and brakes. *Journal of Electrical Engineering*, *3*(3), 379-384. https://doi.org/10.5370/JEET.2008.3.3.379

[10] Sajjad, M., Mojtaba, M., & Heidar, A.T. (2014). Analytical Modeling and Analysis of Axial-flux Interior Permanent-magnet Couplers, *IEEE Transactions on Industrial Electronics*, *61*(11), 5940-5946. https://doi.org/10.1109/TIE.2014.2311391

[11] Lubin, T. & Rezzoug, A. (2015). 3-D Analytical Model for Axial-flux Eddy-current Couplings and Brakes under Steady-state Conditions. *IEEE Transactions on Magnetics*, *51*(10), 1-12. https://doi.org/10.1109/TMAG.2015.2455955

[12] Ge, Y. J., Yuan, Z., & Jia, F. (2016). Mechanical Properties and Testing for Squirrel Cage Asynchronous. *Transactions of the Chinese Society of Agricultural Engineering*, *32*(12), 68-74. https://doi.org/10.11975/j.issn.1002-5819.2016.12.010

[13] Vahid, A., Mirsalim, M., & Rasul, F. (2018). Design Optimization of Double-Sided Permanent-magnet Axial Eddy-current Couplers for Use in Dynamic Applications. *IEEE Transactions on Energy Conversion*, *34*(2), 909-920. https://doi.org/10.1109/TEC.2018.2880679

[14] Yang, C. J., Zhu, L., & Wu, Y. (2021). Speed-control Characteristics of Slotted-Type Axial-flux Asynchronous Magnetic Couplers. *Electric Machines and Control*, *25*(11), 130-138. https://doi.org/10.15938/j.emc.2021.11.015

[15] Yang. J. Y., Wang. D. M., & Ge, Y. J. (2022). Research on Transmission Performance and Experiment of Outer Cage Magnetic Coupling, *UPB Scientific Bulletin, Series D: Mechanical Engineering*, *84*(3), 97-108.

[16] See https://magnadrive.com/industries/applications/
[17] See http://www.magna-drive.com/index.php?m=
home&c=Lists&a=index&tid=166

Contact information:

Junyue YANG
(Corresponding author)
School of Mechanical Engineering,
Dalian Jiaotong University,
794 Huanghe Road,
Shahekou District, Dalian 116028, China
E-mail: xxyykk40@sina.com

Yanjun GE
School of Mechanical Engineering,
Dalian Jiaotong University,
794 Huanghe Road,
Shahekou District, Dalian 116028, China
E-mail: geyanjun1964@126.com